

# MIR503HG silencing promotes endometrial stromal cell progression and metastasis and suppresses apoptosis in adenomyosis by activating the Wnt/ $\beta$ -catenin pathway via targeting miR-191

XIAOPING XU<sup>1\*</sup>, BIN CAI<sup>1\*</sup>, YANG LIU<sup>1</sup>, RUIQIAN LIU<sup>1</sup> and JIA LI<sup>2</sup>

<sup>1</sup>Department of Gynecology, People's Hospital of Deyang City, Deyang, Sichuan 618000; <sup>2</sup>Department of Gynecology, Guizhou Province Maternal and Child Health Hospital, Guiyang, Guizhou 550000, P.R. China

Received June 22, 2021; Accepted December 16, 2022

DOI: 10.3892/etm.2023.11816

**Abstract.** MIR503HG is a 786 bp long lncRNA located on chromosome Xq26.3, and it can regulate diverse cellular processes. The pathogenesis of adenomyosis (AD) is associated with endometrial stromal cells (ESCs). The present study investigated the specific role of MIR503HG in AD pathogenesis and progression using ESCs derived from the endometrium of patients with AD as a model. Expression of MIR503HG and microRNA (miR)-191 were assessed using reverse transcription-quantitative PCR. An immunocytochemistry assay was used to detect cytokeratin- or vimentin-positive ESCs. Transfections of ESCs with MIR503HG overexpression plasmid, short hairpin-MIR503HG and miR-191 inhibitor were performed. ESC viability, migration, invasion and apoptosis were evaluated using Cell Counting Kit-8, Transwell and flow cytometry assays. The association between MIR503HG and miR-191 was predicted by StarBase and confirmed using a dual-luciferase reporter assay. Expression of epithelial-mesenchymal transition-related markers (E-cadherin and N-cadherin) and Wnt/ $\beta$ -catenin pathway-related molecules ( $\beta$ -catenin) in ESCs were analyzed by western blotting. The isolated ESCs were vimentin-positive and cytokeratin-negative. MIR503HG was lowly expressed in the endometrial tissues derived from patients with AD. MIR503HG overexpression hindered ESC viability, migration and invasion while enhancing the apoptosis and downregulating miR-191 expression. MIR503HG knockdown induced the opposite effects, accompanied by downregulation of the E-cadherin expression and upregulation

of N-cadherin and  $\beta$ -catenin levels. MIR503HG directly targeted miR-191 that was highly expressed in endometrial tissues derived from patients with AD. In ESCs, downregulation of miR-191 inhibited the viability, migration and invasion and the expression of N-cadherin and  $\beta$ -catenin levels while enhancing the apoptosis and E-cadherin expression in ESCs. Moreover, downregulation of miR-191 partially reversed the effect of MIR503HG knockdown. Collectively, overexpressed MIR503HG impeded the proliferation and migration of ESCs derived from endometrium of patients with AD, while promoting apoptosis via inhibition of the Wnt/ $\beta$ -catenin pathway via targeting miR-191.

## Introduction

Adenomyosis (AD) is defined as invasion of endometrial glands and stroma into the myometrium (1). Following a limited or diffuse growth pattern, AD develops into endometrial glands in the myometrium (2) and can coexist with endometriosis (3). Manifesting as pelvic pain and abnormal uterine bleeding, AD has a close association with female infertility, dysmenorrhea and dyspareunia (2,4,5). AD is defined as a benign gynecological disease, however, according to some reports, patients with AD may have a risk of malignant transformation (6,7), during which the endometrium invaded by AD can progress into endometrioid adenocarcinoma followed by serous and clear cell carcinoma and poorly differentiated adenocarcinoma, severely threatening health (8). Therefore, early diagnosis and timely treatment are key for suppressing the progression and the malignant transformation of AD. Understanding of the AD condition remains poor despite the upgrade in diagnostic tools (6) and current management of AD still lacks international guidelines (9).

It may be a novel approach to develop the treatment of AD from the perspective of genetics, as long non-coding RNAs (lncRNAs) are aberrantly expressed in both eutopic and ectopic endometria of patients with AD (10,11). Classified as a subgroup of ncRNAs, lncRNAs are >200 nucleotides in length and possess regulatory effects on AD progression (12-14). Placenta-enriched lncRNA MIR503 host gene (MIR503HG), located on chromosome Xq26.3 where genes associated with

---

*Correspondence to:* Dr Xiaoping Xu, Department of Gynecology, People's Hospital of Deyang City, 173 Section 1 Taishan North Road, Jingyang, Deyang, Sichuan 618000, P.R. China  
E-mail: xuxiaopp\_xxp@163.com

\*Contributed equally

**Key words:** MIR503HG, adenomyosis, endometrial stromal cell, microRNA-191, Wnt/ $\beta$ -catenin pathway

human reproduction are enriched (15), is highly expressed and associated with unfavorable outcomes in endometrial cancer (16) and preeclampsia (17), but is lowly expressed and suppresses tumor growth by inhibiting cell migration and invasion in triple-negative breast cancer (18). However, the specific expression and mechanism of MIR503HG in AD remain unclear.

In addition, the conventional view is that AD results from the abnormal down-growth and invagination of the endometrium into the myometrium (19). Studies have reported that lncRNA-mediated inhibition of proliferation and enhancement of apoptosis in endometrial stromal cells (ESCs) ameliorates AD (12-14). Meanwhile, at only ~22 nucleotides in length and also classified as ncRNAs, microRNAs (miRNAs or miRs) have been discovered to act as a downstream mechanism of lncRNA-mediated changes in processes of ESCs during AD progression (13). Among them, miR-191 is notably dysregulated in the endometrium tissues of patients with AD (20). Therefore, identifying downstream miRNAs of lncRNAs that regulate AD is key.

In the present study, the expression of MIR503HG in AD was characterized and a potential mechanism by which MIR503HG regulates AD by modulating its downstream miRNAs was investigated. Meanwhile, since MIR503HG has been reported to target miR-191 to promote tumor inhibition in cervical cancer (21), further experiments were performed to determine their roles in AD.

## Materials and methods

**Ethics approval.** The study was ratified by the Ethics Committee of People's Hospital of Deyang City (approval no. GD202000524; Deyang, China) and written informed consent from all participants was obtained for experimental work involving tissues obtained from humans.

**Clinical samples.** AD tissue (n=30) was collected from the endometrium of patients with AD (mean age, 42.75±5.62 years; range, 31-58 years) who had been diagnosed clinically and pathologically at People's Hospital of Deyang City in July 2020 to November 2020. None of the patients had received preoperative chemotherapy, radiotherapy or hormone therapy or had a history of chronic disease such as coronary heart disease and hypertension. During the same period, specimens taken from the endometrium (n=30) of patients with cervical lesions or uterine fibroids after hysterectomy but without AD (mean age, 40.24±3.73 years; range, 32-49 years) were used as the control group. In the control group, the patients had no history of hormone therapy or chronic diseases. All tissues were immediately snap-frozen in liquid nitrogen at -80°C for 40 min for further use.

**Isolation, identification and culture of ESCs.** ESCs were isolated from the endometrium of patients with AD (n=3) as follows: The endometrium was cut into 0.5-1.0 mm<sup>3</sup> sections and digested with 0.25% trypsin (cat. no. 9002-07-7; Sigma-Aldrich; Merck KGaA) that was diluted to 1.25 mg/l with Dulbecco's Modified Eagle Medium (DMEM)/F-12 (cat. no. 21041025; Thermo Fisher Scientific, Inc.). The sections were incubated at 37°C with 5% CO<sub>2</sub> for 80 min, then a cell

suspension was obtained and filtered twice through a nylon mesh (140- and 37- $\mu$ m mesh in sequence). Subsequently, the filtered suspension was centrifugated at 1,000 x g for 5 min at 4°C and ESCs were obtained as previously described (22). When the confluence of ESCs was 90% under an optical microscope (BX50; Olympus Corporation; magnification, x200), ESCs were maintained in DMEM/F12 (50 ml), supplemented with 10% fetal bovine serum (FBS; cat. no. F2442), 2 mmol glutamine (cat. no. 1294808) and 1% penicillin-streptomycin (cat. no. P4333; all Sigma-Aldrich; Merck KGaA) at 37°C with 5% CO<sub>2</sub>.

**Immunocytochemistry assay.** After being fixed in 4% paraformaldehyde (cat. no. P6148; Sigma-Aldrich; Merck KGaA) for 15 min at room temperature, ESCs (2x10<sup>4</sup> cells/ml) were washed with PBS (cat. no. P5493, Sigma-Aldrich; Merck KGaA) three times and incubated with 0.1% Triton X-100 (cat. no. X100; Sigma-Aldrich; Merck KGaA) for improvement of permeability. The cells were washed with PBS three times and blocked in 5% bovine serum albumin (cat. no. A7030; Sigma-Aldrich; Merck KGaA) for 20 min at room temperature. Subsequently, anti-vimentin (cat. no. PA5-27231; 1:1,000; Thermo Fisher Scientific, Inc.) and anti-cytokeratin antibody (cat. no. PA5-32465; 1:100; Thermo Fisher Scientific, Inc.) were used to incubate the cells at 4°C overnight. After being washed with PBS, cells were incubated with goat anti-Rabbit IgG HRP (cat. no. 31466; 1:1,000; Thermo Fisher Scientific, Inc.) at 4°C for 60 min in the dark. Following washing with PBS, cells were color-developed using diaminobenzidine (cat. no. D8001; Sigma-Aldrich; Merck KGaA) for 5 min at room temperature and counterstained with hematoxylin (cat. no. H3136, Sigma-Aldrich; Merck KGaA) for 1 min at room temperature. ESCs were observed by a light microscope (IX71; Olympus Corporation; magnification, x200).

**Cell transfection.** MIR503HG overexpression plasmids were constructed with pcDNA3.1 vector (cat. no. V79520; Thermo Fisher Scientific, Inc.). Short hairpin (sh)-MIR503HG (5'-CATCCAGCATCTCCAGTTA-3') was constructed using MISSION pLKO.1-puro Empty Vectors (cat. no. SHC001; Sigma-Aldrich; Merck KGaA). Empty vector and scrambled sequence (5'-TTCTCCGAACGTGTCACGT-3') were used as negative controls (NCs). miR-191 inhibitor/inhibitor control (IC; miR20000440-1-5, 5'-CAGCUGCUUUGGGAUUCGGUUG-3'; miR2N0000001-1-5, 5'-UCUACU CUUUCUAGGAGGUUGUGA-3') and mimic/mimic control (miR10000440-1-5, 5'-CAACGGAAUCCCAAAGCAGCUG-3'; miR1N0000001-1-5, 5'-UUCUCCGAACGUGUCACGU-3') were purchased from Guangzhou RiboBio Co., Ltd. ESCs were transfected with MIR503HG overexpression plasmids, sh-MIR503HG, miR-191 inhibitor/mimic or a combination of sh-MIR503HG and miR-191 inhibitor using Lipofectamine 3000<sup>®</sup> (cat. no. L3000015; Thermo Fisher Scientific, Inc.). Briefly, ESCs were plated in 96-well plates at a density of 1x10<sup>4</sup> cells/well and cultured to 80% confluence. Opti-MEM (10  $\mu$ l; cat. no. 31985062; Thermo Fisher Scientific, Inc.) and P3000 reagents (0.4  $\mu$ l; Thermo Fisher Scientific, Inc.) were used in combination to dilute the plasmids (0.2  $\mu$ g) and Lipofectamine 3000 (0.15  $\mu$ l), and the diluted Lipofectamine 3000 reagent and diluted plasmid was mixed,

followed by incubation at 37°C for 10 min. Finally, RNA-lipid complex was added to 96-well plates to incubate the cells at 37°C for 24 or 48 h before further use.

**Dual-luciferase reporter assay.** Starbase v.2.0 (<https://starbase.sysu.edu.cn/>) was used to predict the targeting association between MIR503HG and miR-191. Wild-type (WT; 5'-ATGCTGCTTTT-GATTTCCGT TA-3') and mutant (MUT; 5'-ATGCTGACTTT-GAT TTCCGTTA-3') MIR503HG 3'-untranslated region were cloned into pmirGLO vectors (cat. no. E1330, Promega Corporation) to synthesize pMirGLO-MIR503HG-WT and pMirGLO-MIR503HG-MUT, respectively. ESCs were plated into 12-well plates at a density of  $1 \times 10^7$  cells/well and cultured to 70% confluence at 37°C. The cells were co-transfected with miR-191 mimic (100 ng) and pmirGLO vectors (100 ng) inserted with fragments of MIR503HG WT or MUT sequence using Lipofectamine 3000® (Thermo Fisher Scientific, Inc.) at 37°C for 48 h. Dual-luciferase reporter assay was immediately performed with Dual-Luciferase Reporter Assay System (cat. no. E1980, Promega Corporation). Firefly luciferase activity, normalized to *Renilla* luciferase activity and measured using a luminometer (GloMax® 20/20; Promega Corporation), was used to express the binding specificity.

**RNA immunoprecipitation (RIP) assay.** RIP assay was performed using a RIP kit (cat. no. RIP-12RXN; Sigma-Aldrich; Merck KGaA). ESCs were digested with trypsin (Sigma-Aldrich; Merck KGaA) and collected the cells, and then cells were transferred into a mixed solution containing PBS, nuclear separation buffer and double-distilled H<sub>2</sub>O. The solution was stirred on ice and centrifuged at  $2,500 \times g$  for 15 min at 4°C. The precipitated nucleus of ESCs was resuspended in RIP buffer. The solution was uniformly divided into IgG and the Ago2 group. The supernatant in the IgG group was added to 10 µg anti-IgG antibody (cat. no. ab171870; 1:1,000; Abcam) while that in the Ago2 group was added to 10 µg Ago2 antibody (cat. no. ab186733; 1:30; Abcam), gently shaken and then incubated at 4°C overnight. The supernatant was added to 40 µl protein A/G magnetic beads (cat. no. M2400; Beijing Solarbio Science & Technology Co., Ltd.) and cultured at 4°C for 1 h. Unconjugated protein was removed by RIP buffer washing. The untreated cell lysate was used as an input group. The RNAs in the input group, IgG and Ago2 group were extracted and reverse-transcribed into cDNA. Subsequently, the expression of miR-191 and MIR503HG were measured via quantitative polymerase chain reaction (qPCR). Expression in the input group was considered to be positive control.

**Cell Counting Kit (CCK)-8 assay.** Following transfection, ESCs were plated into 96-well plates at a density of  $5 \times 10^3$  cells/well. CCK-8 reagent (cat. no. C0037; Beyotime Institute of Biotechnology) was added into the cells at a ratio of 1:10, after which cell incubation was performed at 37°C for 1 h. Cell viability was measured based on the optical density using a microplate reader (Synergy Neo2; BioTek Instruments, Inc.; Agilent Technologies, Inc.) at a wavelength of 450 nm.

**Transwell assay.** Cell migration and invasion of transfected ESCs were evaluated by Transwell chambers (cat. no. 428; Corning, Inc.). For invasion assays, Transwell upper chambers were precoated with Matrigel (cat. no. 356234; Corning, Inc.) diluted at a ratio of 1:3 and incubated at 37°C for 2 h. Following transfection, ESCs were suspended in serum-free DMEM/F12 to a concentration of  $2 \times 10^5$  cells/ml and cell suspension (100 µl) was poured into the upper chamber. The lower chamber was filled with DMEM/F12 (600 µl) supplemented with 10% FBS (cat. no. F2442; Sigma-Aldrich; Merck KGaA). The whole Transwell chamber was incubated at 37°C for 24 h, after which non-migratory or non-invading cells in the upper chamber were removed. The remaining cells were washed twice with PBS, fixed in 4% paraformaldehyde (cat. no. P6148; Sigma-Aldrich; Merck KGaA) at room temperature for 20 min and stained with Giemsa (800 µl; cat. no. 10092013; Thermo Fisher Scientific, Inc.) at room temperature for 15 min. Finally, stained cells were observed under an inverted light microscope (IX71; Olympus Corporation) and counted with ImageJ v.1.47 (National Institutes of Health, Bethesda, MD, USA) from eight randomly selected fields. The cell migration or invasion rate was set to 100% in control groups, while that in other groups was calculated by comparing the mean cell number with that in the control group.

**Flow cytometry.** The apoptosis of transfected ESCs was measured using Annexin V-FITC/PI apoptosis detection kit (cat. no. 40302ES20; Shanghai Yeasen Biotechnology Co., Ltd.). After transfection, ESCs were digested in EDTA-free trypsin (cat. no. T2600000; Sigma-Aldrich; Merck KGaA) at room temperature for 2 min and centrifugated at  $3,000 \times g$  for 5 min at 4°C, followed by washing with PBS. Subsequently, the cells were resuspended with 1X Binding Buffer to reach the concentration of  $1 \times 10^6$  cells/ml. Annexin V-FITC solution (5 µl) and PI solution (10 µl) were used to incubate the cells in the dark for 10 min at room temperature. Apoptotic cells (early and late apoptosis) were examined using a flow cytometer (CytoFLEX; Beckman Coulter, Inc.) and analyzed with CytExpert software (Version 2.2.0.97; Beckman Coulter, Inc.).

**Reverse transcription-(RT)qPCR.** AD tissues were homogenized using a UH-05 homogenizer (Union-Biotech). Total RNA and miRNA were extracted from ESCs, with or without transfection and AD and control tissues using TRIzol® (cat. no. 15596026; Thermo Fisher Scientific, Inc.) and PureLink miRNA Isolation kit (cat. no. K157001; Thermo Fisher Scientific, Inc.), respectively. The extracted total RNA and miRNA were reverse-transcribed to cDNA using SuperScript IV reverse transcriptase (cat. no. 18090010; Thermo Fisher Scientific, Inc.) according to the manufacturer's protocol. qPCR was performed on a CFX Connect Real-Time PCR Detection System (Bio-Rad Laboratories, Inc.) using PowerUp SYBR Green Master Mix (cat. no. A25742; Thermo Fisher Scientific, Inc.). The primer pairs used for qPCR are listed in Table I. The thermocycling conditions were as follows: Initial denaturation at 95°C for 10 min; 40 cycles of annealing at 95°C for 15 sec and elongation at 60°C for 60 sec. Quantification was performed using the 2<sup>-ΔΔC<sub>q</sub></sup> method (23) and the expression levels of MIR503HG were normalized to GAPDH while miR-191 was normalized to U6.

Table I. Human primers used for reverse transcription-quantitative PCR.

Gene	Forward, 5'→3'	Reverse, 5'→3'
MIR503HG	CTTGAAGGCATCCAGCATCTC	TTGGGACACTTGGGTGGTTTT
microRNA-191	CGGAATCCCAAAGCAGCTG	TGTCGTGGAGTCGGCAATTG
GAPDH	GAGAAGGCTGGGGCTCATTT	AGTGATGGCATGGACTGTGG
U6	CTCGCTTCGGCAGCACA	AACGCTTCACGAATTTGCGT

**Western blotting.** Total protein from transfected ESCs was extracted using RIPA Buffer (cat. no. 89900; Thermo Fisher Scientific, Inc.) and quantified using a BCA assay (cat. no. A53227; Thermo Fisher Scientific, Inc.). The extracted protein (40 µg/lane) and marker (4 µl; cat. no. PR1910; Beijing Solarbio Science & Technology Co., Ltd.) were loaded and separated by SDS-PAGE on a 10 or 12% gel (cat. nos. P0670 and P0672, Beyotime Institute of Biotechnology) and then transferred onto PVDF membranes (cat. no. P2438; Sigma-Aldrich; Merck KGaA). The membranes were blocked with 5% non-fat milk in TBS with 1% Tween-20 (TBST; cat. no. T9039, Sigma-Aldrich; Merck KGaA) for 1 h at 37°C. Subsequently, membranes were incubated with primary antibodies against E-cadherin (cat. no. ab40772; 97 kDa; 1:10,000; Abcam), N-cadherin (cat. no. ab18203; 130 kDa; 1:1,000; Abcam), β-catenin (cat. no. 9562; 92 kDa, 1:1,000; Cell Signaling Technology, Inc.), cleaved caspase-3 (cat. no. ab32042; 17 kDa; 1:500; Abcam) and GAPDH (cat. no. 5174; 37 kDa; 1:1,000; Cell Signaling Technology, Inc.) at 4°C overnight. Following washing with TBST, membranes were incubated with a secondary Goat anti-Rabbit IgG Alexa Fluor™ Plus 488 (cat. no. A32731; 1:10,000; Thermo Fisher Scientific, Inc.) at 37°C for 1 h. Immunoreactive bands were visualized using enhanced chemiluminescence reagent kit (cat. no. WP20005; Thermo Fisher Scientific, Inc.) on an imaging device (iBright CL750; Thermo Fisher Scientific, Inc.) and analyzed using ImageJ Software (1.52s version; National Institutes of Health).

**Statistical analysis.** All statistical analyses were conducted with GraphPad Prism (version 8.0; GraphPad Software Inc.). Data were obtained from independent experiments performed in triplicate and are presented as mean ± standard deviation. Differences between two groups were analyzed using the unpaired Student's t test, while those between multiple groups were analyzed using one-way analysis of variance followed by Tukey's post hoc test. P<0.05 was considered to indicate a statistically significant difference.

## Results

**MIR503HG is lowly expressed in AD tissue and regulates viability, migration, invasion and apoptosis in ESCs derived from the endometrium of patients with AD.** RT-qPCR demonstrated that the MIR503HG expression in AD tissues was much lower than that in tissues collected from patients with cervical lesions or uterine fibroids (P<0.001; Fig. 1A). The physiological and pathological characteristics of ESCs isolated from the endometrium of patients with AD were investigated. Morphological examination via an optical microscope of

isolated ESCs revealed that ESCs derived from patients with AD were polygons with an elliptical nucleus that was primarily located at the center of the cell and had noticeable nucleoli (Fig. 1B). In addition, immunocytochemistry assay illustrated that the cytoplasm of the ESCs was positive for vimentin with brownish yellow, but was negative for cytokeratin with purplish red nuclei (Fig. 1C). To investigate the role of MIR503HG in AD, isolated ESCs were subjected to transfection with MIR503HG overexpression plasmids or sh-MIR503HG; MIR503HG was successfully overexpressed and knocked down (P<0.001; Fig. 1D), respectively. CCK-8 and Transwell assays were performed to detect the viability, migration and invasion rates of ESCs derived from patients with AD; these were confirmed to be significantly decreased by MIR503HG overexpression (P<0.01 for viability and P<0.001 for both migration and invasion vs. NC; Fig. 1E-I) and increased by MIR503HG knockdown (P<0.05, P<0.01 and P<0.001 vs. NC, respectively; Fig. 1F-I). Moreover, flow cytometry analysis showed that apoptosis of ESCs was promoted by MIR503HG overexpression but inhibited by MIR503HG knockdown (P<0.001; Fig. 1J and K).

**MIR503HG is a sponge of miR-191 and inhibits miR-191 expression in ESCs derived from patients with AD while miR-191 is highly expressed in AD tissues.** Starbase bioinformatics analysis demonstrated that miR-191 had binding sites with MIR503HG (Fig. 2A). Dual-luciferase reporter assay was performed, the result of which showed that with transfection of miR-191 mimic, luciferase activity of ESCs derived from patients with AD and transfected with pMirGLO-MIR503HG-WT was suppressed (P<0.001; Fig. 2B), while that of cells transfected with pMirGLO-MIR503HG-MUT remained unchanged (Fig. 2B). RIP assay demonstrated that the expression levels of both miR-191 and MIR503HG were increased in the anti-Ago2 group, indicating binding of miR-191 and MIR503HG (P<0.001 vs. IgG; Fig. 2C). RT-qPCR showed that miR-191 expression was downregulated by MIR503HG overexpression but upregulated by MIR503HG knockdown in ESCs derived from patients with AD (P<0.001; Fig. 2D), while high expression of miR-191 was observed in AD tissue (P<0.001; Fig. 2E).

**miR-191 inhibition partially reversed the effect of MIR503HG knockdown on the AD-derived ESC viability and migration/invasion and apoptosis.** miR-191 inhibitor was introduced to determine the role of miR-191 in the MIR503HG-associated effects on ESCs derived from patients with AD. According to RT-qPCR results, expression of miR-191 was significantly decreased after ESCs were transfected with miR-191 inhibitor (P<0.001; Fig. 3A) and upregulation of miR-191 was observed

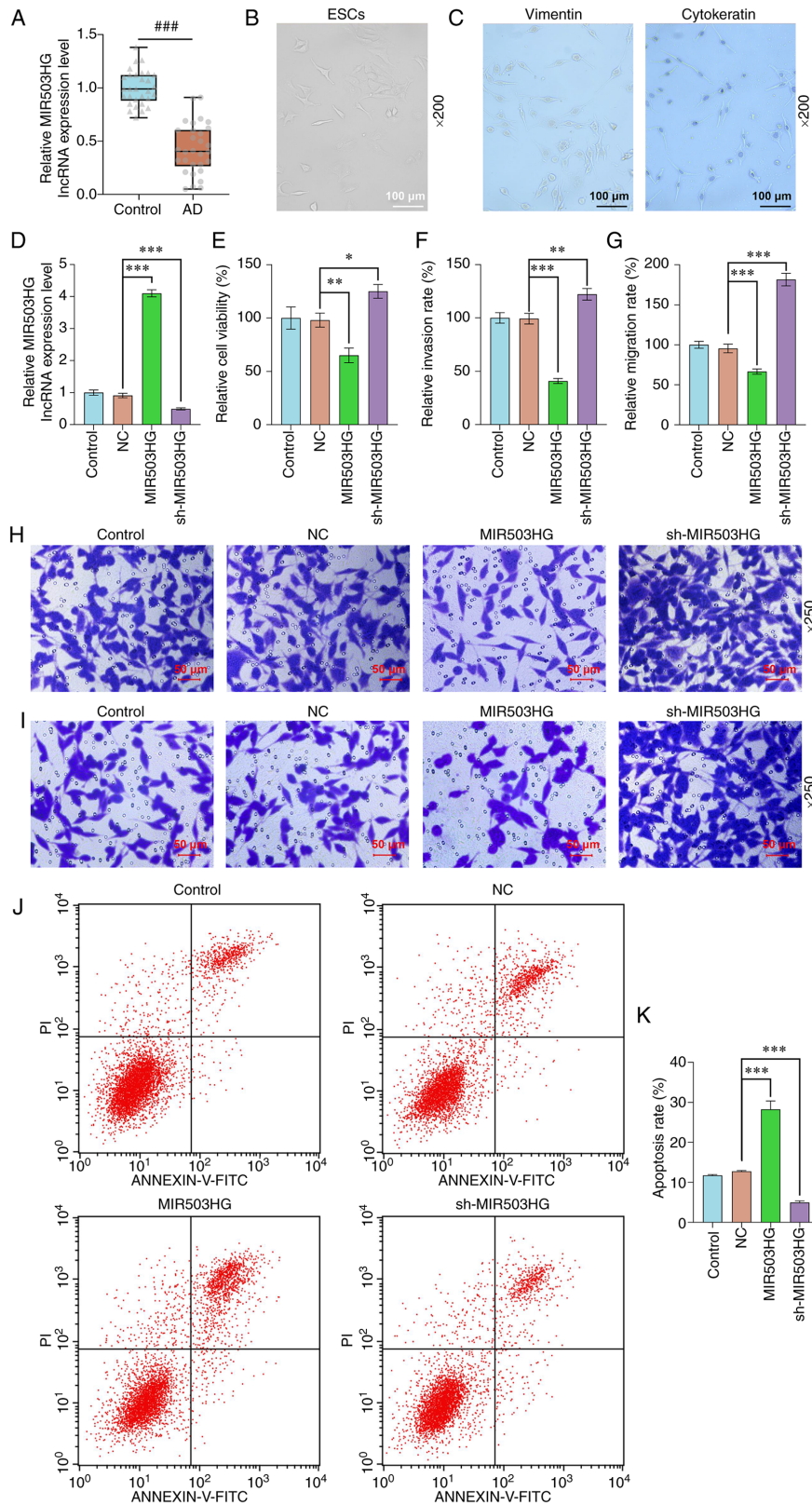


Figure 1. MIR503HG is lowly expressed in AD tissue and regulates viability, migration, invasion and apoptosis in ESCs derived from patients with AD. (A) Expression of MIR503HG in the endometrium of patients with AD or cervical lesions/uterine fibroids was analyzed using RT-qPCR. (B) ESCs isolated from AD tissue were observed under an optical microscope (scale bar, 100  $\mu$ m). (C) Cytokeratin and vimentin expression in ESCs was assessed via immunocytochemistry (scale bar, 100  $\mu$ m). (D) Expression of MIR503HG in ESCs derived from patients with AD transfected with MIR503HG overexpression plasmids/sh-MIR503HG was analyzed using RT-qPCR. (E) Viability of ESCs derived from patients with AD transfected with MIR503HG overexpression plasmids/sh-MIR503HG was measured via Cell Counting Kit-8 assay. (F) Invasion and (G) migration rate of ESCs derived from patients with AD transfected with MIR503HG overexpression plasmids/sh-MIR503HG were evaluated. (H) Invasion and (I) migration of ESCs transfected with MIR503HG overexpression plasmids/sh-MIR503HG was detected via Transwell assay (scale bar, 50  $\mu$ m). (J) Apoptosis of ESCs derived from patients with AD transfected with MIR503HG overexpression plasmid/sh-MIR503HG was measured via flow cytometry. (K) Apoptosis rate of ESCs was quantified. \* $P < 0.05$ , \*\* $P < 0.01$  and \*\*\* $P < 0.001$  vs. NC. ### $P < 0.001$  vs. control. AD, adenomyosis; ESCs, endometrial stromal cells; RT-q, reverse transcription-quantitative; NC, negative control; sh, short hairpin; Inc, long non-coding.

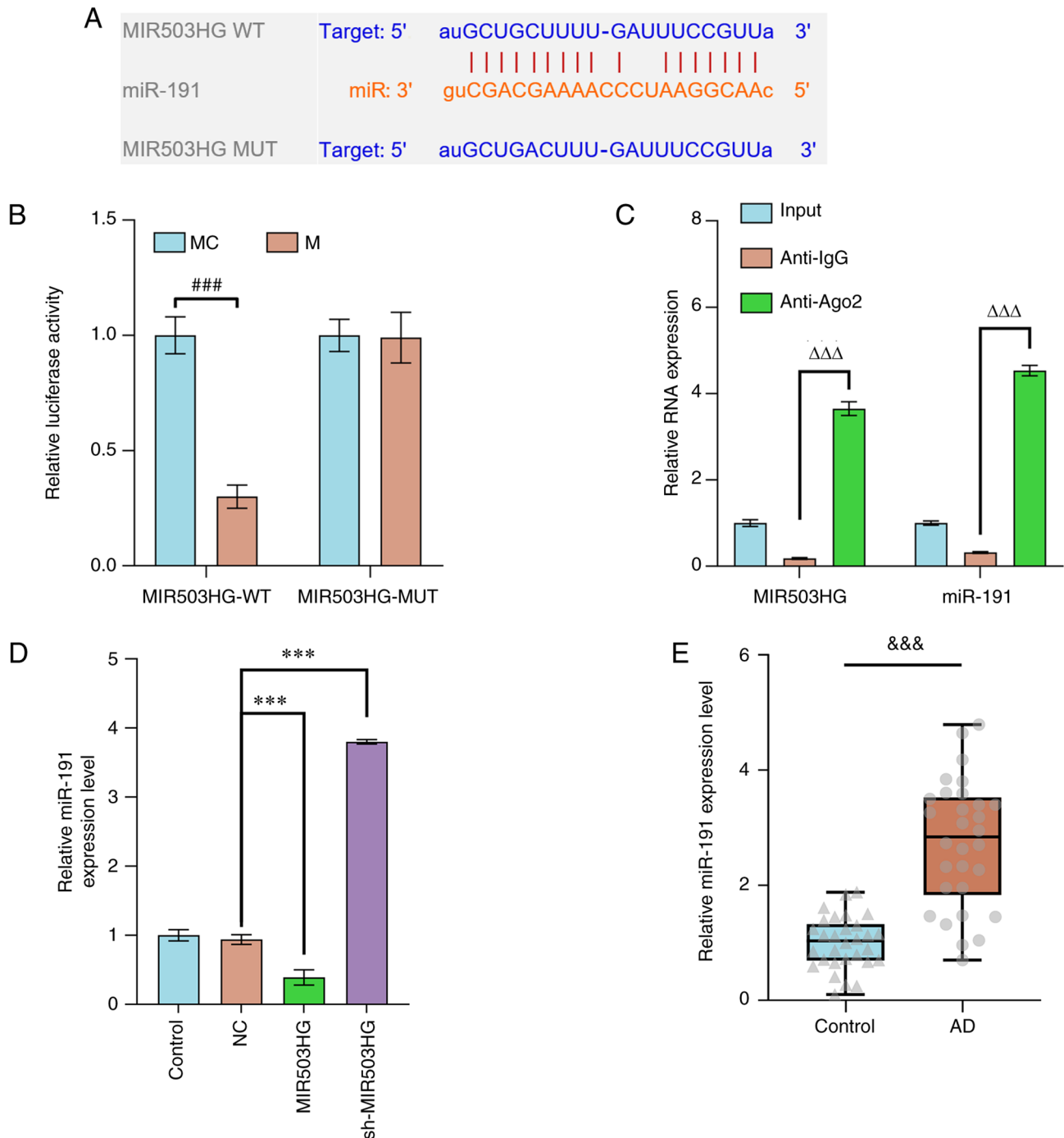


Figure 2. miR-191 is highly expressed in AD tissue and is directly targeted and negatively regulated by MIR503HG in ESCs derived from patients with AD. (A) Binding sites of miR-191 on MIR503HG WT were predicted by StarBase. (B) miR-191 was confirmed as a target miR of MIR503HG by dual-luciferase reporter assay. (C) RNA immunoprecipitation assay validated the co-expression of miR-191 with MIR503HG. The expression of miR-191 in (D) ESCs derived from patients with AD transfected with sh-MIR503HG or MIR503HG overexpression plasmids and (E) endometrium from patients with AD or cervical lesions or uterine fibroids was analyzed via RT-qPCR. ###P<0.001 vs. MC. \*\*\*P<0.001 vs. NC. &&&P<0.001 vs. control. ΔΔΔP<0.001 vs. anti-IgG. AD, adenomyosis; ESCs, endometrial stromal cells; RT-q, reverse transcription-quantitative; M, miR-191 mimic; MC, mimic control; WT, wild-type; MUT, mutant; NC, negative control; miR, microRNA.

following MIR503HG knockdown (P<0.001; Fig. 3B), and miR-191 inhibitor reversed MIR503HG knockdown-induced upregulation of miR-191 (P<0.001; Fig. 3B). CCK-8, Transwell and flow cytometry assay results demonstrated that miR-191 inhibition decreased the viability and the migration and invasion rates of ESCs derived from patients with AD and augmented the apoptosis rate (P<0.001 vs. NC + IC; Fig. 3C-I). MIR503HG knockdown promoted the viability

and the migration and invasion of ESCs derived from patients with AD and inhibited the apoptosis (P<0.01, P<0.001 vs. NC + IC; Fig. 3C-I). In addition, miR-191 inhibition attenuated the effect of MIR503HG knockdown on viability and migration, invasion and apoptosis of ESCs derived from patients with AD (P<0.001; Fig. 3C-3I). Moreover, cleaved caspase-3 was used as the indicator of apoptosis and its expression was decreased by MIR503HG knockdown (P<0.001;

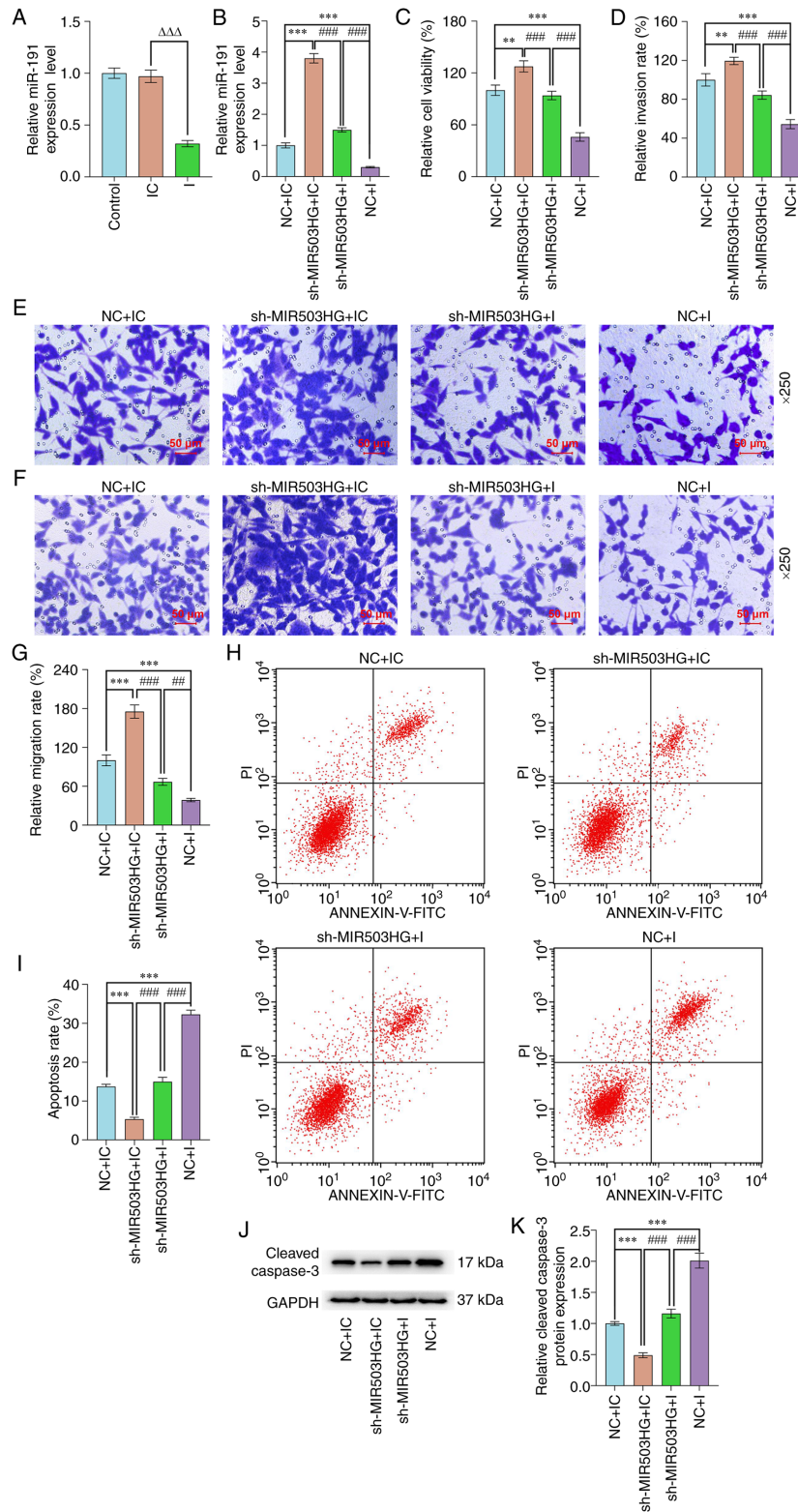


Figure 3. miR-191 inhibition partially reversed the effect of MIR503HG knockdown on the viability and migration/invasion and apoptosis in ESCs derived from patients with AD potentially. (A) Expression of miR-191 in ESCs derived from patients with AD that were transfected with I was analyzed via RT-qPCR. (B) Expression of miR-191 in ESCs derived from patients with AD transfected with sh-MIR503HG or I alone or in combination was analyzed via RT-qPCR. (C) Viability of ESCs derived from patients with AD transfected with sh-MIR503HG or I alone or in combination was measured via Cell Counting Kit-8 assay. (D) Invasion rate of ESCs derived from patients with AD transfected with sh-MIR503HG or I alone or in combination was quantified. (E) Invasion of ESCs derived from patients with AD transfected with sh-MIR503HG or I alone or in combination were evaluated via Transwell assay (scale bar, 50  $\mu$ m). (F) Migration of ESCs derived from patients with AD transfected with sh-MIR503HG or I alone or in combination were evaluated via Transwell assay (scale bar, 50  $\mu$ m). (G) Migration rate of ESCs derived from patients with AD transfected with sh-MIR503HG or I alone or in combination was quantified. (H) Apoptosis of ESCs derived from patients with AD transfected with sh-MIR503HG or I alone or in combination was measured via flow cytometry. (I) Apoptosis rate of ESCs was quantified. (J) Expression of cleaved caspase-3 in ESCs derived from patients with AD transfected with sh-MIR503HG or I alone or in combination was measured by western blotting with GAPDH as reference gene. (K) Protein expression of cleaved caspase-3 in ESCs was quantified.  $\Delta\Delta\Delta P < 0.001$  vs. IC.  $**P < 0.01$  and  $***P < 0.001$  vs. NC + IC.  $##P < 0.01$   $###P < 0.001$  vs. sh-MIR503HG + I. AD, adenomyosis; ESC, endometrial stromal cell; RT-q, reverse transcription-quantitative; I, miR-191 inhibitor; IC, inhibitor control; NC, negative control; miR, microRNA; sh, short hairpin.

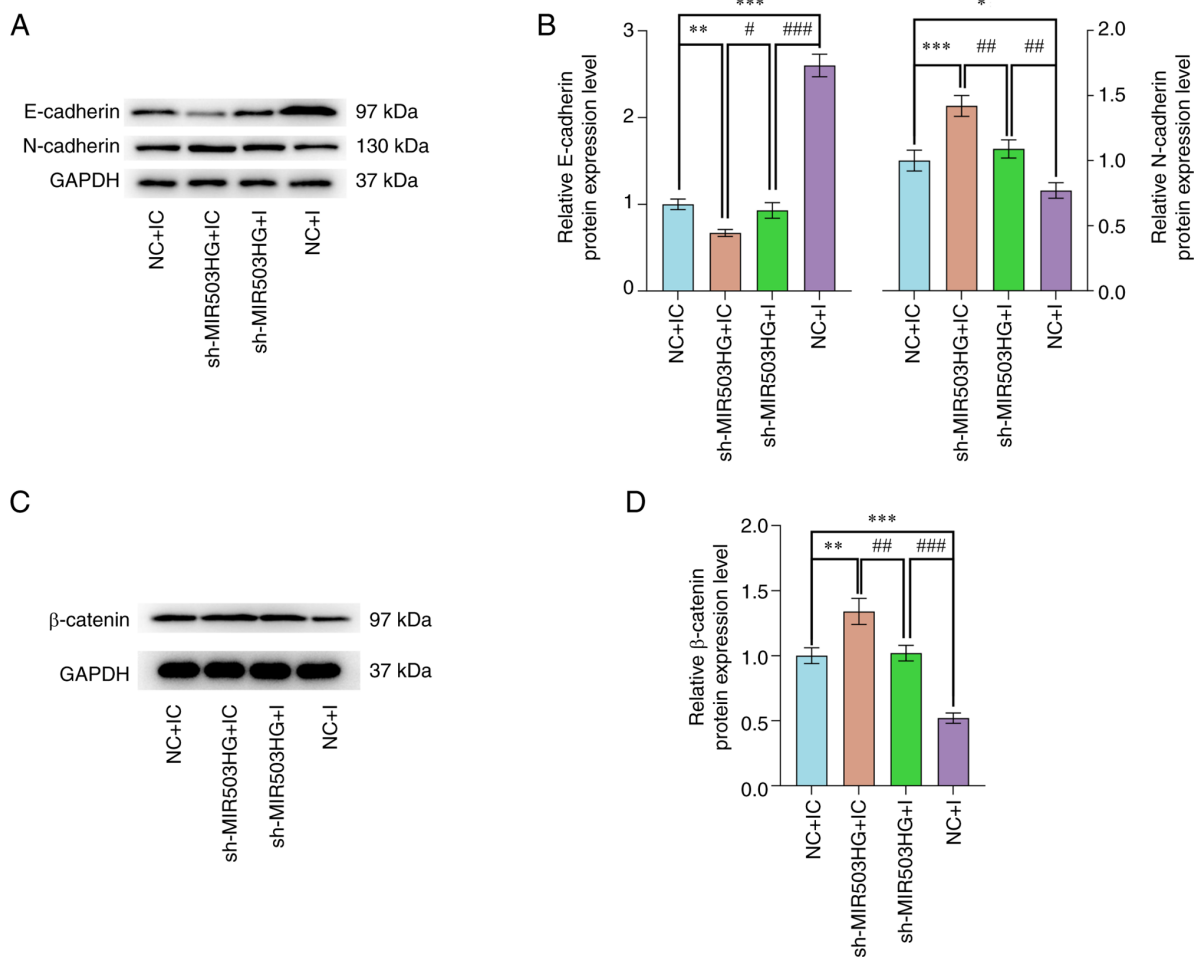


Figure 4. MIR503HG knockdown promotes epithelial-mesenchymal transition and activates the Wnt/ $\beta$ -catenin pathway by reversing miR-191 inhibition in ESCs derived from patients with AD. (A) Expression of E-cadherin and N-cadherin in ESCs derived from patients with AD transfected with sh-MIR503HG or I alone or in combination was detected by western blotting. (B) Protein expression of E-cadherin and N-cadherin in ESCs was quantified. (C) Expression of  $\beta$ -catenin in ESCs derived from patients with AD transfected with sh-MIR503HG or I alone or in combination were analyzed by western blotting with GAPDH as the reference gene. (D) Protein expression of  $\beta$ -catenin in ESCs was quantified. \* $P < 0.01$ , \*\* $P < 0.05$  and \*\*\* $P < 0.001$  vs. NC + IC. # $P < 0.05$ , ## $P < 0.01$  and ### $P < 0.001$  vs. sh-MIR503HG + I. AD, adenomyosis; ESCs, endometrial stromal cells; RT-q, reverse transcription-quantitative; I, miR-191 inhibitor; IC, inhibitor control; NC, negative control; sh, short hairpin; miR, microRNA.

Fig. 3J and K) but increased by miR-191 inhibitor in ESCs ( $P < 0.001$ ; Fig. 3J and K). Moreover, miR-191 inhibitor attenuated the effect of MIR503HG knockdown on the expression of cleaved caspase-3 ( $P < 0.001$ ; Fig. 3J and K).

*MIR503HG knockdown facilitates epithelial-mesenchymal transition (EMT) and activates the Wnt/ $\beta$ -catenin pathway by regulating miR-191 expression in ESCs derived from patients with AD.* A previous study demonstrated that EMT is a cellular process key for miR-191 upregulation-promoted cancer progression (24). In addition, the Wnt/ $\beta$ -catenin pathway is one of the underlying mechanisms of EMT in AD (25). Western blotting showed that MIR503HG knockdown significantly downregulated the levels of E-Cadherin and upregulated those of N-cadherin and  $\beta$ -catenin ( $P < 0.01$ ,  $P < 0.001$  and  $P < 0.01$  vs. NC + IC, respectively; Fig. 4A-D), while miR-191 inhibition significantly upregulated the levels of E-Cadherin and downregulated those of N-cadherin and  $\beta$ -catenin ( $P < 0.001$ ,  $P < 0.05$  and  $P < 0.001$  vs. NC + IC, respectively; Fig. 4A-D). Moreover, miR-191 inhibition attenuated the effect of MIR503HG knockdown on levels of E-cadherin,

N-cadherin and  $\beta$ -catenin ( $P < 0.05$ ,  $P < 0.01$  and  $P < 0.001$ , vs. sh-MIR503HG + IC, respectively; Fig. 4A-D).

## Discussion

Although no direct evidence has indicated that AD triggers infertility, AD interferes with the success of *in vitro* fertilization (26). Prolonged treatment time of AD can result not only in placental dislocation, preeclampsia and premature delivery, but also cause endometrial adenocarcinoma (7,27,28). Currently, AD, as a common benign pathology, is asymptomatic in one-third of cases (29) and diagnostic indices for AD are still lacking (6). There is no early classification of the extent of the disease (30) and biomarkers need to be discovered for the management of AD.

Aberrantly expressed lncRNAs, which have been proposed to serve as diagnostic and therapeutic markers in assorted diseases, such as cancer, cardiovascular disease and osteoarthritis, have been detected in patients with AD (10,11). MIR503HG has been previously identified as key in sustaining endothelial cell biology and angiogenic processes (31) and

is highly expressed in the placenta and other reproductive tissues (32). As AD refers to invasion of the endometrium into the myometrium, it is reasonable to hypothesize that MIR503HG is lowly expressed in patients with AD; this was confirmed in AD tissue in the present study.

ESCs are closely associated with the pathogenesis of AD, and inhibited ESC proliferation contributes to AD progression (13). Previous studies have demonstrated that transition of ESCs to epithelial cells suppresses AD progression (33) and resistance to the apoptosis of ESCs may account for the pathogenesis of AD (22). Moreover, inhibition of proliferation, migration and enhancement of apoptosis are considered a radically and efficiently conservative method for the treatment of AD (22). Overexpression of MIR503HG in preeclampsia-derived trophoblast cells inhibits cell proliferation, migration and invasion, which underly the pathogenesis of preeclampsia (17). MIR503HG overexpression leads to enhanced apoptosis of high glucose-cultured human proximal tubular (HK-2) cells (34). Contrary to the role of MIR503HG in preeclampsia but consistent with that in high glucose-induced HK-2 cells, the present study demonstrated that overexpression of MIR503HG impeded the viability, migration and invasion and enhanced the apoptosis of ESCs isolated successfully from the endometrial tissue of patients with AD. In addition, the pathogenesis of AD is affected by EMT (33). EMT is characterized by epithelial cells obtaining mesenchymal phenotypes through undergoing loss of cell polarity, remodeling of the cytoskeleton, acquired invasiveness and resistance to apoptosis (35,36). During this process, E-cadherin (an epithelial marker) expression is downregulated and N-cadherin (a mesenchymal marker) expression is upregulated (37). The present study demonstrated that the knockdown of MIR503HG led to downregulated E-cadherin and upregulated N-cadherin, indicating that MIR503HG overexpression may reverse EMT during AD progression. Overall, the present findings demonstrated that restoration of MIR503HG expression may help suppress AD progression.

Eutopic endometrium of patients with AD exhibits reciprocally dysregulated miRNAs such as upregulated miR-191, the analysis of which may be a promising low-invasive method for efficient diagnosis of AD (20). In addition, miRNAs participate in lncRNA-mediated AD progression by serving as the downstream targets of lncRNAs (13). The present study identified that miR-191 was directly targeted by MIR503HG and enriched in AD tissue, which is in line with its expression in adipose-derived mesenchymal stem cells that have stromal features (38). In addition, inhibition of miR-191 reversed the MIR503HG knockdown-induced the viability, migration, invasion increased and apoptosis decreased in ESCs derived from patients with AD to suppress AD progression, which signified that inhibition of AD progression induced by restoration of MIR503HG expression was miR-191 inhibition-dependent.

Additionally, a previous study discovered that the activation of the Wnt/ $\beta$ -catenin signaling pathway contributes to the pathogenesis of AD via EMT (39). In the nucleus of epithelial cells, functioning as the main effector of the canonical Wnt signaling which initiates EMT,  $\beta$ -catenin is key for tissue differentiation during embryonic development (39) and elevated  $\beta$ -catenin levels indicate activation of Wnt/ $\beta$ -catenin signaling (25). By analyzing  $\beta$ -catenin

expression, the present study demonstrated that the Wnt/ $\beta$ -catenin pathway was activated by MIR503HG knockdown but suppressed by miR-191 inhibition, which also reversed MIR503HG knockdown-induced Wnt/ $\beta$ -catenin activation, denoting that the MIR503HG/miR-191 axis-mediated amelioration of AD resulted from inhibited Wnt/ $\beta$ -catenin signaling.

In conclusion, the present findings demonstrated that MIR503HG was lowly expressed in AD, and MIR503HG exerted a suppressive impact on AD progression by targeting miR-191, which was enriched in ESCs derived from patients with AD, to decrease viability, migration, invasion and EMT while enhancing apoptosis. This suppression may involve inhibition of the Wnt/ $\beta$ -catenin pathway. The present study provided new insights into the therapeutic strategies for AD. However, examinations in a clinical situation or peripheral blood samples were not performed to elucidate the role of MIR503HG or miR-191 in survival or prognosis of patients with AD. Also, the size of samples was small. In addition, the analysis of Wnt/ $\beta$ -catenin signaling pathway in future studies requires MIR503HG overexpression and rescue experiments.

#### Acknowledgements

Not applicable.

#### Funding

The present study was supported by the Deyang Science and Technology Bureau (grant no. 2020SZZ078).

#### Availability of data and materials

The datasets used and/or analyzed during the current study are available from the corresponding author on reasonable request.

#### Authors' contributions

XX and BC provided substantial contributions to conception and design and wrote and revised the manuscript. YL, RL and JL performed data acquisition, analysis and interpretation. All authors have read and approved the final manuscript. XX and BC confirm the authenticity of all the raw data.

#### Ethics approval and consent to participate

The present study was approved by the ethics committee of People's Hospital of Deyang City (approval no. GD202000524) and written informed consent from all participants was obtained for experiments involving tissue.

#### Patient consent for publication

Not applicable.

#### Competing interests

The authors declare that they have no competing interests.

## References

1. Ferenczy A: Pathophysiology of adenomyosis. *Hum Reprod Update* 4: 312-322, 1998.
2. Lacheta J: Uterine adenomyosis: Pathogenesis, diagnostics, symptomatology and treatment. *Ceska Gynecol* 84: 240-246, 2019.
3. Leyendecker G, Bilgicyildirim A, Inacker M, Stalf T, Huppert P, Mall G, Böttcher B and Wildt L: Adenomyosis and endometriosis. Re-visiting their association and further insights into the mechanisms of auto-traumatisation. An MRI study. *Arch Gynecol Obstet* 291: 917-932, 2015.
4. Harada T, Khine YM, Kaponis A, Nikellis T, Decavalas G and Taniguchi F: The impact of adenomyosis on women's fertility. *Obstet Gynecol Surv* 71: 557-568, 2016.
5. Peric H and Fraser IS: The symptomatology of adenomyosis. *Best Pract Res Clin Obstet Gynaecol* 20: 547-555, 2006.
6. Vannuccini S and Petraglia F: Recent advances in understanding and managing adenomyosis. *F1000Res* 8: F1000, 2019.
7. Khalifa MA, Atri M, Klein ME, Ghatak S and Murugan P: Adenomyosis as a confounder to accurate endometrial cancer staging. *Semin Ultrasound CT MR* 40: 358-363, 2019.
8. Yuan H and Zhang S: Malignant transformation of adenomyosis: Literature review and meta-analysis. *Arch Gynecol Obstet* 299: 47-53, 2019.
9. Vannuccini S, Luisi S, Tosti C, Sorbi F and Petraglia F: Role of medical therapy in the management of uterine adenomyosis. *Fertil Steril* 109: 398-405, 2018.
10. Jiang JF, Sun AJ, Xue W, Deng Y and Wang YF: Aberrantly expressed long noncoding RNAs in the eutopic endometria of patients with uterine adenomyosis. *Eur J Obstet Gynecol Reprod Biol* 199: 32-37, 2016.
11. Zhou C, Zhang T, Liu F, Zhou J, Ni X, Huo R and Shi Z: The differential expression of mRNAs and long noncoding RNAs between ectopic and eutopic endometria provides new insights into adenomyosis. *Mol Biosyst* 12: 362-370, 2016.
12. Bhan A, Soleimani M and Mandal SS: Long noncoding RNA and cancer: A new paradigm. *Cancer Res* 77: 3965-3981, 2017.
13. Liang N, Zhang W, Wang H, Shi W, Wang L and Ma L: Levonorgestrel ameliorates adenomyosis via lncRNA H19/miR-17/TLR4 pathway. *Drug Des Devel Ther* 14: 3449-3460, 2020.
14. Xu XY, Zhang J, Qi YH, Kong M, Liu SA and Hu JJ: Linc-ROR promotes endometrial cell proliferation by activating the PI3K-Akt pathway. *Eur Rev Med Pharmacol Sci* 22: 2218-2225, 2018.
15. Fiedler J, Baker AH, Dimmeler S, Heymans S, Mayr M and Thum T: Non-coding RNAs in vascular disease—from basic science to clinical applications: scientific update from the working group of myocardial function of the European Society of Cardiology. *Cardiovasc Res* 114: 1281-1286, 2018.
16. Tang H, Wu Z, Zhang Y, Xia T, Liu D, Cai J and Ye Q: Identification and function analysis of a five-long noncoding RNA prognostic signature for endometrial cancer patients. *DNA Cell Biol* 38: 1480-1498, 2019.
17. Cheng D, Jiang S, Chen J, Li J, Ao L and Zhang Y: The increased lncRNA MIR503HG in preeclampsia modulated trophoblast cell proliferation, invasion, and migration via regulating matrix metalloproteinases and NF- $\kappa$ B signaling. *Dis Markers* 2019: 4976845, 2019.
18. Fu J, Dong G, Shi H, Zhang J, Ning Z, Bao X, Liu C, Hu J, Liu M and Xiong B: LncRNA MIR503HG inhibits cell migration and invasion via miR-103/OLFM4 axis in triple negative breast cancer. *J Cell Mol Med* 23: 4738-4745, 2019.
19. Parrott E, Butterworth M, Green A, White IN and Greaves P: Adenomyosis—a result of disordered stromal differentiation. *Am J Pathol* 159: 623-630, 2001.
20. Borisov E, Knyazeva M, Novak V, Zabegina L, Prisyazhnaya T, Karizkiy A, Berlev I and Malek A: Analysis of reciprocally dysregulated miRNAs in eutopic endometrium is a promising approach for low invasive diagnostics of adenomyosis. *Diagnostics (Basel)* 10: 782, 2020.
21. Hu YL, Zhang YX, Liu N, Liu H and Yuan YC: LncRNA MIR503HG regulated cell viability, metastasis and apoptosis of cervical cancer via miR-191/CEBPB axis. *Eur Rev Med Pharmacol Sci* 25: 3200-3210, 2021.
22. Li J, Yanyan M, Mu L, Chen X and Zheng W: The expression of Bcl-2 in adenomyosis and its effect on proliferation, migration, and apoptosis of endometrial stromal cells. *Pathol Res Pract* 215: 152477, 2019.
23. Livak KJ and Schmittgen TD: Analysis of relative gene expression data using real-time quantitative PCR and the 2(-Delta Delta C(T)) method. *Methods* 25: 402-408, 2001.
24. Xu W, Ji J, Xu Y, Liu Y, Shi L, Liu Y, Lu X, Zhao Y, Luo F and Wang B: MicroRNA-191, by promoting the EMT and increasing CSC-like properties, is involved in neoplastic and metastatic properties of transformed human bronchial epithelial cells. *Mol Carcinog* 54 (Suppl 1): E148-E161, 2015.
25. Feng T, Wei S, Wang Y, Fu X, Shi L, Qu L and Fan X: Rhein ameliorates adenomyosis by inhibiting NF- $\kappa$ B and  $\beta$ -Catenin signaling pathway. *Biomed Pharmacother* 94: 231-237, 2017.
26. Vercellini P, Bonfanti I and Berlanda N: Adenomyosis and infertility: Is there a causal link? *Expert Rev Endocrinol Metab* 14: 365-367, 2019.
27. Hashimoto A, Iriyama T, Sayama S, Nakayama T, Komatsu A, Miyachi A, Nishii O, Nagamatsu T, Osuga Y and Fujii T: Adenomyosis and adverse perinatal outcomes: Increased risk of second trimester miscarriage, preeclampsia, and placental malposition. *J Matern Fetal Neonatal Med* 31: 364-369, 2018.
28. Shin YJ, Kwak DW, Chung JH, Kim MY, Lee SW and Han YJ: The risk of preterm births among pregnant women with adenomyosis. *J Ultrasound Med* 37: 1937-1943, 2018.
29. Aleksandrovych V, Basta P and Gil K: Current facts constituting an understanding of the nature of adenomyosis. *Adv Clin Exp Med* 28: 839-846, 2019.
30. Dueholm M: Uterine adenomyosis and infertility, review of reproductive outcome after in vitro fertilization and surgery. *Acta Obstet Gynecol Scand* 96: 715-726, 2017.
31. Fiedler J, Breckwoldt K, Remmele CW, Hartmann D, Dittrich M, Pfanne A, Just A, Xiao K, Kunz M, Müller T, *et al*: Development of long noncoding RNA-based strategies to modulate tissue vascularization. *J Am Coll Cardiol* 66: 2005-2015, 2015.
32. Muys BR, Lorenzi JC, Zanette DL, Lima e Bueno Rde B, de Araújo LF, Dinarte-Santos AR, Alves CP, Ramão A, de Molfetta GA, Vidal DO and Silva WA Jr: Placenta-enriched lincRNAs MIR503HG and LINC00629 decrease migration and invasion potential of JEG-3 cell line. *PLoS One* 11: e0151560, 2016.
33. Li Y, Zhang Q, Liu F, Zhang Z, Zou Y, Yang B, Luo Y, Wang L and Huang O: Inhibition of formin like 2 promotes the transition of ectopic endometrial stromal cells to epithelial cells in adenomyosis through a MET-like process. *Gene* 710: 186-192, 2019.
34. Cao X and Fan QL: LncRNA MIR503HG promotes high-glucose-induced proximal tubular cell apoptosis by targeting miR-503-5p/Bcl-2 pathway. *Diabetes Metab Syndr Obes* 13: 4507-4517, 2020.
35. Lee JM, Dedhar S, Kalluri R and Thompson EW: The epithelial-mesenchymal transition: new insights in signaling, development, and disease. *J Cell Biol* 172: 973-981, 2006.
36. Yang J and Weinberg RA: Epithelial-mesenchymal transition: At the crossroads of development and tumor metastasis. *Dev Cell* 14: 818-829, 2008.
37. Zheng D, Duan H, Wang S, Xu Q, Gan L, Li J and Dong Q: FAK regulates epithelial-mesenchymal transition in adenomyosis. *Mol Med Rep* 18: 5461-5472, 2018.
38. Zhang C, Wang P, Mohammed A, Zhou Z, Zhang S, Ni S and Tang Z: Function of adipose-derived mesenchymal stem cells in monocrotaline-induced pulmonary arterial hypertension through miR-191 via regulation of BMPR2. *Biomed Res Int* 2019: 2858750, 2019.
39. Oh SJ, Shin JH, Kim TH, Lee HS, Yoo JY, Ahn JY, Broaddus RR, Taketo MM, Lydon JP, Leach RE, *et al*:  $\beta$ -Catenin activation contributes to the pathogenesis of adenomyosis through epithelial-mesenchymal transition. *J Pathol* 231: 210-222, 2013.



This work is licensed under a Creative Commons Attribution-NonCommercial-NoDerivatives 4.0 International (CC BY-NC-ND 4.0) License.